pISSN 2384-1095
eISSN 2384-1109

iMRI 2022;26:104-116

https://doi.org/10.13104/imri.2022.26.2.104

iMRI
Investigative Magnetic Resonance Imaging

Percentile-Based Analysis of Non-Gaussian Diffusion Parameters for Improved Glioma Grading

M. Muge Karaman[1,2], Christopher Y. Zhou[3], Jiaxuan Zhang[1,4], Zheng Zhong[1,2], Kezhou Wang[1], Wenzhen Zhu[4]

[1]Center for MR Research, University of Illinois at Chicago, Chicago, IL, USA
[2]Department of Biomedical Engineering, University of Illinois at Chicago, Chicago, IL, USA
[3]Trinity College, Duke University, Durham, NC, USA
[4]Department of Radiology, Tongji Hospital, Tongji Medical College, Huazhong University of Science and Technology, Wuhan, Hubei, China

Original Article

Received: October 28, 2021
Revised: March 18, 2022
Accepted: May 17, 2022

Correspondence to:
M. Muge Karaman, Ph.D.
Center for Magnetic Resonance Research, University of Illinois at Chicago; 2242 West Harrison Street, Suite 103, M/C 831, Chicago, IL 60612, USA.
Tel. +1-312-413-7849
Fax. +1-312-355-1637
E-mail: mkaraman@uic.edu

The purpose of this study is to systematically determine an optimal percentile cut-off in histogram analysis for calculating the mean parameters obtained from a non-Gaussian continuous-time random-walk (CTRW) diffusion model for differentiating individual glioma grades. This retrospective study included 90 patients with histopathologically proven gliomas (42 grade II, 19 grade III, and 29 grade IV). We performed diffusion-weighted imaging using 17 b-values (0-4000 s/mm^2) at 3T, and analyzed the images with the CTRW model to produce an anomalous diffusion coefficient (D_m) along with temporal (α) and spatial (β) diffusion heterogeneity parameters. Given the tumor ROIs, we created a histogram of each parameter; computed the P-values (using a Student's t-test) for the statistical differences in the mean D_m, α, or β for differentiating grade II vs. grade III gliomas and grade III vs. grade IV gliomas at different percentiles (1% to 100%); and selected the highest percentile with $P < 0.05$ as the optimal percentile. We used the mean parameter values calculated from the optimal percentile cut-offs to do a receiver operating characteristic (ROC) analysis based on individual parameters or their combinations. We compared the results with those obtained by averaging data over the entire region of interest (i.e., 100th percentile). We found the optimal percentiles for D_m, α, and β to be 68%, 75%, and 100% for differentiating grade II vs. III and 58%, 19%, and 100% for differentiating grade III vs. IV gliomas, respectively. The optimal percentile cut-offs outperformed the entire-ROI-based analysis in sensitivity (0.761 vs. 0.690), specificity (0.578 vs. 0.526), accuracy (0.704 vs. 0.639), and AUC (0.671 vs. 0.599) for grade II vs. III differentiations and in sensitivity (0.789 vs. 0.578) and AUC (0.637 vs. 0.620) for grade III vs. IV differentiations, respectively. Percentile-based histogram analysis, coupled with the multi-parametric approach enabled by the CTRW diffusion model using high b-values, can improve glioma grading.

Keywords: Glioma; Glioma grading; Non-Gaussian diffusion-weighted imaging, Continuous-time random-walk model; Histogram analysis; High b value

INTRODUCTION

Gliomas are the most common primary intracranial neoplasm, with a broad range of clinical manifestations. According to the 2016 WHO central nervous system (CNS) tumor classifications (1), gliomas are classified into four grades ranging from grade I to grade IV, with increasing aggressiveness and malignancy. Traditionally, grade I and II gliomas are termed low grade; and have a better prognosis. Grade III and IV gliomas, on the other hand, are considered high -grade because of their invasiveness and poor prognosis (2). The WHO classifications of gliomas have always included grading as a malignancy scale, even with the recent introduction of robust molecular markers, such as isocitrate dehydrogenase 1 and 2 (IDH1 and IDH2), 1p/19q, and O[6]-methylguanine-DNA methyltransferase (MGMT) (1, 3). Traditional grading combined with modern molecular markers can account for differences in the biological properties of gliomas, providing valuable information about prognoses and responses to therapies.

The current gold standard for glioma grading is based on histopathologic and molecular evaluation of surgical biopsy or resection specimens (1). Over the past decades, magnetic resonance imaging (MRI) has been widely used for the preoperative assessment of gliomas due to their ability to noninvasively evaluate the entire spatial extent of the lesion, including the adjacent brain tissues. Besides morphologic, perfusion, and/or spectroscopic MRI sequences, diffusion-weighted MRI (DWI) has been increasingly incorporated into the clinical MRI protocols for assessing gliomas to improve the diagnostic accuracy (4-8). In particular, the apparent diffusion coefficient (ADC) from DWI has been employed to differentiate low-grade from high-grade gliomas (9). Although simple and useful, an ADC derived from a mono-exponential model assumes that the diffusion-driven displacements of water molecules follow a Gaussian distribution (10). In biological tissues, however, the diffusion displacement distribution deviates from Gaussian distribution, and a DWI signal cannot be adequately characterized by a mono-exponential function (11, 12). To characterize this non-Gaussian diffusion behavior, many advanced DWI models have been proposed (13-28). Among these are the continuous-time random-walk (CTRW) model (26, 29) and its predecessor, the fractional order calculus (FROC) model, both of which have improved the characterization of DWI signals in a high b-value regime (30-32). In earlier studies, the CTRW and FROC model parameters were found to be sensitive to microscopic tissue structural heterogeneity at a sub-voxel level, particularly in tumor tissues (23-26, 30-33).

Irrespective of the diffusion model employed, most studies have relied on region-of-interest (ROI) analyses, which compute the mean value of diffusion parameters over the tumor tissues. However, the voxel values of diffusion parameters within a tumor can differ widely, primarily because of macroscopic tissue heterogeneity, resulting in under- or over-estimation (34). Recognizing the high degree of intra-tumor heterogeneity, some investigators have recently employed percentile-based histogram analysis in DWI studies (35-39). Using the distribution of relevant diffusion parameters, this approach can provide multiple quantitative metrics beyond the mean value, thus providing opportunities for improved characterization of intra-tumoral heterogeneity and identification of the most diagnostic tissue components in a manner similar to that of histopathological analysis. When a percentile-based analysis is used, a key issue is to establish a percentile cutoff. Using a small percentage (e.g., 5%) may reduce the statistical power of the analysis and cause it to miss important tissue components, whereas using a large percentage (e.g., 90%) may reduce the sensitivity because of the averaging effect among heterogenous tissues and can be subject to the same limitations caused by using the mean value from the entire ROI. Our goal in this study is to systematically and statistically determine an optimal percentile cut-off for calculating the mean parameters obtained from a CTRW model for differentiating between individual glioma grades.

MATERIALS AND METHODS

Patients

This retrospective study was approved by the local Institutional Review Board, and all patients gave written-informed consent to the study. Glioma patients were included based on the following criteria: (1) age ≥ 18 years; (2) no history of treatment; (3) availability of data from multi b-value DWI and routine MRI; and (4) histopathologic confirmation of the tumor in accordance with the WHO guidelines. The exclusion criteria included (1) excessive artifacts in the MR images; (2) diameter of the tumor's short axis < 3 cm; or (3) the time between the MRI scan and surgical resection or biopsy > 2 weeks. Using these criteria, 91 subjects were included in the study, consisting of 1 grade I, 42 grade II, 19 grade III, and 29 grade IV gliomas. The single patient with a grade I glioma was excluded from

analysis because of the small sample size. The mean age of the remaining participants (39 females and 51 males) was 44.1 years ± 12.6 (standard deviation) with an age range of 18-75 years.

Image Acquisition

Prior to surgical resection or biopsy, all patients were scanned on a 3T General Electric MR750 scanner (General Electric Healthcare, Waukesha, WI, USA) with a commercial 32-channel head coil. The MRI protocol included pre-contrast transverse T1 fluid-attenuated inversion recovery (T1-FLAIR), T2 fast spin echo (T2-FSE), T2-FLAIR, and multi-b-value DWI, followed by post-contrast T1-FLAIR. The acquisition parameters for DWI were: TR/TE = 700/100 ms, section thickness = 5 mm, inter-section spacing = 1.5 mm, separation between two diffusion gradient lobes Δ = 38.6 ms, duration of each diffusion gradient lobe δ = 32.2 ms, FOV (field of view) = 22 × 22 cm^2, matrix size = 256 × 256, and 17 b values = 0_1, 20_1, 50_1, 100_1, 200_1, 400_1, 600_1, 800_1, 1000_1, 1200_1, 1600_1, 2000_2, 2400_2, 2800_2, 3200_4, 3600_4, and 4000_4 s/mm^2 (where the subscripts represent the number of averages). The total scan time for DWI was 4 minutes and 16 seconds to obtain 20 slices covering the whole brain. To mitigate the effect of diffusion anisotropy, we applied the diffusion-weighting gradient successively along the three orthogonal directions, producing a trace-weighted image for analysis (40).

Diffusion Image Analysis

A CTRW model was employed to fit to the multi-b-value diffusion-weighted images according to Equation [1] (26):

$$S/S_0 = E_\alpha [-(bD_m)^\beta], \quad [1]$$

where D_m is an anomalous diffusion coefficient, α and β are parameters related to temporal and spatial diffusion heterogeneities, respectively, and E_α is a Mittag-Leffler function. The CTRW parameter maps of D_m, α, and β were generated by nonlinear least-squares fitting, which used an iterative Levenberg-Marquardt algorithm in Matlab (MathWorks, Inc., Natick, MA, USA). After noise rejection and Rician noise correction (23), the fitting proceeded by first estimating D_m using the diffusion images with b-values ≤ 2800 s/mm^2, followed by a simultaneous estimation of α and β from all diffusion-weighted images (b-values = 0 - 4000 s/mm^2) using a function value termination tolerance of 10^{-4} and limiting the number of iterations to 100.

Percentile-Based Histogram Analysis

The ROIs containing the entire tumor, including necrotic or cystic areas, were drawn on b = 0 s/mm^2 images by the consensus of two radiologists who were blinded to histopathological diagnosis. These ROIs were applied to each map of D_m, α, and β for all tumor-containing sections, producing a volume of interest for each glioma patient, which were then analyzed by using a histogram to determine the percentile cut-offs, as described below. After the patients were separated by their glioma grades, we performed a statistical analysis for each CTRW parameter. To better illustrate the processing steps, we will use the α parameter as an example.

First, a histogram of α was created based on the voxel values within the full volume of interest for each patient. Second, starting from the left tail of the histogram (i.e., from the lower α values), each percentile between 1% and 100% was investigated as a cut-off to calculate the mean α value. At each percentile cut-off, the α values within that percentile were averaged using an arithmetic mean. Third, for each percentile cut-off, a Student's t-test was used to calculate the P-value for the statistical difference in the mean α between grade II and III and between grade III and IV gliomas. Finally, we defined the optimal percentile cut-offs for each differentiation (i.e., grade II vs. III and grade III vs. IV gliomas) as being the greatest percentile cut-offs that yielded a P-value less than 0.05. The rationale behind this choice was that more data would yield greater statistical power. This same procedure was repeated for the remaining two CTRW parameters, D_m and β, to determine their optimal percentile cut-off values.

Statistical Analysis

We performed a receiver operator characteristic (ROC) analysis to differentiate the glioma grades. After determining the optimal percentile cut-off for each individual parameter (D_m, α, or β), we computed the optimal mean parameter values by using the values that fell within the percentile cut-off (i.e., between 0% and the percentile cut-off). Using this mean value, we performed an ROC analysis to evaluate each individual parameter's performance in differentiating grade II vs. III and grade III vs. IV gliomas. We also performed an ROC analysis based on the different combinations of the CTRW parameters, (D_m, α), (D_m, β), (α, β), and (D_m, α, β), by using a multivariable logistic regression for each parameter combination, as expressed in Equation [2]

$$P_0 = \exp(a_0 + a_1 D_m + a_2 \alpha + a_3 \beta) / [1 + \exp(a_0 + a_1 D_m + a_2 \alpha + a_3 \beta)], \quad [2]$$

where a_0 is a constant, and a_i (I = 1, 2, 3) are the regression coefficients of the three CTRW parameters.

We compared the performances of the CTRW parameters, individually or jointly, in differentiating the glioma grades by using the sensitivity and specificity cut-off values, the diagnostic accuracy, and the area under the curve (AUC). For comparison, we repeated the ROC analyses based on both the individual parameter and combined parameters by using the conventional approach based on the mean from the entire ROI (i.e., using the 100th percentile as the "cut-off"). Afterwards, we compared the optimal percentile-based analysis with the entire ROI-based analysis, looking for statistical differences in their sensitivity, specificity, and accuracy achieved by the individual CTRW parameters and their combinations , by employing a McNemar test (41) for paired binomial responses. In addition, we compared the AUCs from the two analyses using a Hanley and McNeil test (42).

RESULTS

Figure 1 shows D_m, α, and β maps from three representative patients, one from each of the grade II, III, and IV groups. The tumor ROIs are outlined in black contours in the parameter maps. The CTRW parameter values in the tumor ROIs progressively decreased as the tumor grade increased. Furthermore, these progressive decreases were prominent in only some parts of the heterogeneous ROI, thereby supporting the use of a percentile-based analysis.

Figure 2 shows a representative histogram of D_m values generated from the tumor ROIs of a grade II glioma patient. The optimal percentile for grades II vs. III differentiation is shown as a red vertical line. All data to the right of this line were excluded from the calculation of the mean parameter value.

Figure 3 show the plots of P-value versus percentile cut-off for D_m, α, and β, respectively, for the comparisons of grade II vs. III (in blue) and grade III vs. IV gliomas (in orange). These P-value plots monotonically increased past the third percentile, indicating that inclusion of a large portion of the histogram decreases the statistical significance (i.e., a higher P-value). On the other hand, the P-value at low percentiles (e.g., the 5th percentile for D_m) exhibited greater statistical significance (i.e., a lower P-value) but was determined using fewer data points and was thus subject to unreliability and bias. Both of these observations support the use of a percentile-based histogram analysis.

For grades II vs. III differentiation, we found the percentile cut-off for D_m to be the 68th percentile. The P values based on α were statistically significant up to the 75th percentile. For β, P-value was less than 0.05 at all percentiles. For grades III vs. IV differentiation, the percentile cut-offs for D_m and α were at the 58th and 19th percentiles, respectively. Similar to the separation between grades II and III, P-value for β was less than 0.05 at all percentiles. Overall, the optimal percentiles were generally higher for comparisons between grades II and III than for comparisons between grades III and IV. When the entire ROI (i.e., 100th percentile) was used for calculating the mean parameter values, the differences between grades II and III or grades III and IV were statistically insignificant in D_m (P = 0.202 for grades II vs. III and P = 0.085 for grades III vs. IV) and α (P = 0.132 for grades II vs. III and P = 0.424 for grades III vs. IV).

Figure 4 and Table 1 show the ROC curves and the sensitivity, specificity, accuracy, and AUC of using individual

Table 1. Receiver Operating Characteristic Performance Metrics of Each CTRW (Continuous-time random-walk) Parameter for Grades II and III Differentiation Using an Optimal Percentile-based Histogram Analysis and the Entire-ROI-Based (i.e., 100th Percentile) Analysis

	Optimal percentile-based histogram analysis		
	D_m	α	β
Sensitivity	0.578	0.789	0.684
Specificity	0.690*	0.571	0.667
Accuracy	0.655*	0.639	0.672
AUC	0.634*	0.635*	0.713
	Entire-ROI-based analysis		
Sensitivity	0.578	0.684	0.684
Specificity	0.547*	0.571	0.667
Accuracy	0.557*	0.606	0.672
AUC	0.567*	0.590*	0.713

Analysis in the upper half of the table is based on the mean parameter values computed from the an optimal percentile as described in the text. Analysis in the lower half of the table is based on the mean parameter values computed from the entire ROI.

Asterisk (*) indicates statistical significance between the performance metrics obtained from the optimal percentile- and entire-ROI-based analysis according to the McNemar test for specificity, sensitivity, and accuracy and the Hanley and McNeil test for AUC.

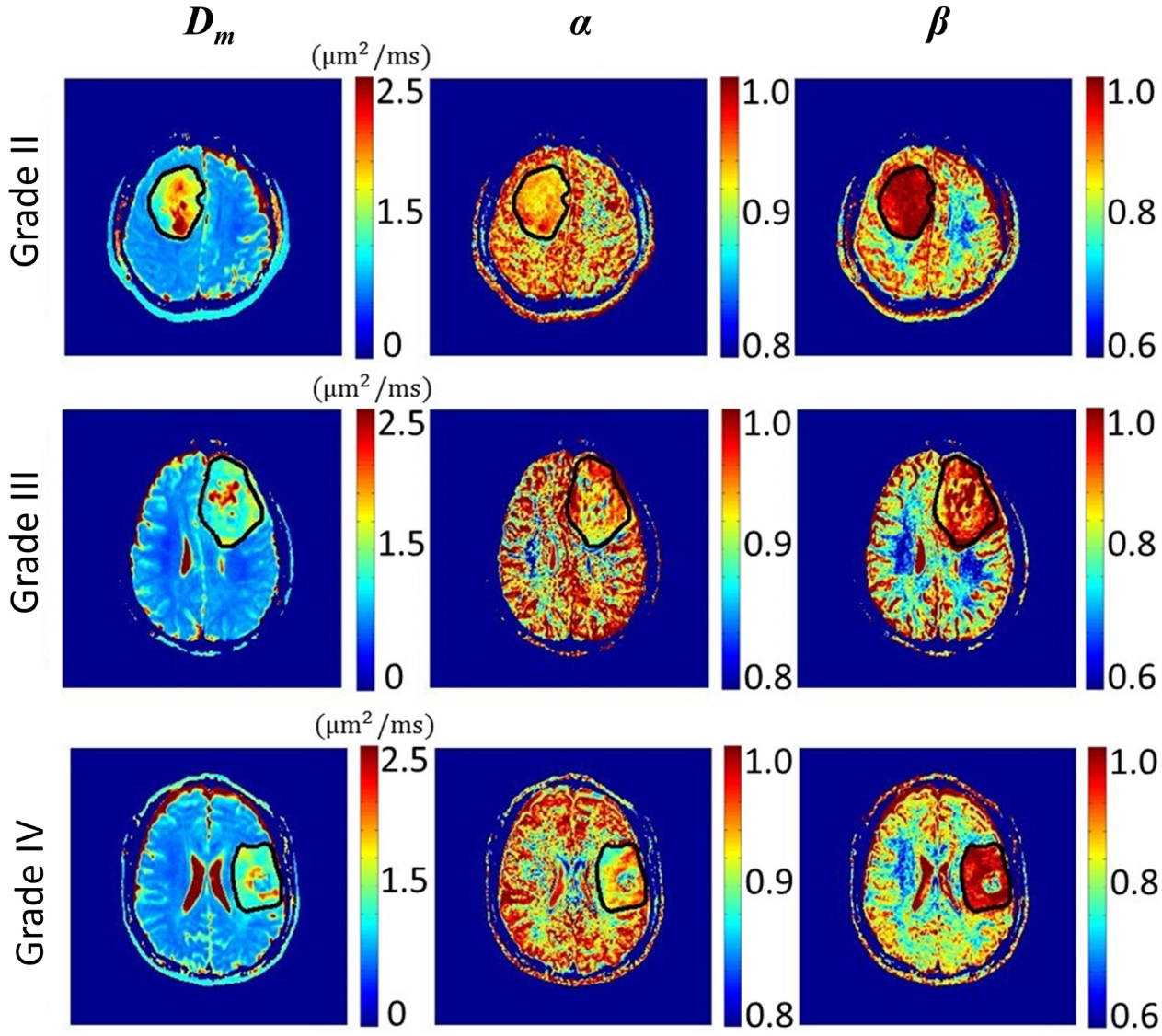

Fig. 1. The maps of CTRW parameters for representative patients in grades II, III, and IV glioma groups. The ROI of each tumor is outlined within the black contours.

parameters, D_m (Fig. 4a), α (Fig. 4b), or β (Fig. 4c), for the separation between grade II and III gliomas. In all cases, the curves obtained from using the optimal percentile cut-off either performed better, with statistically significant differences in most cases, or performed equally as well as the curves obtained from the entire ROI analysis. Overall, α had the best sensitivity (0.789), D_m had the best specificity (0.690), and β had the best accuracy (0.672) and AUC (0.713).

Figure 5 and Table 2 summarize the ROC curves and the sensitivity, specificity, accuracy, and AUC resulting from the use of individual parameters D_m (Fig. 5a), α (Fig. 5b), or β (Fig. 5c), for the separation between grade III and IV gliomas. The results were similar to those from the differentiation between grade II and III gliomas, though we observed improvements in D_m and α's specificity and AUC and α's accuracy when using the optimized percentile cut-off as opposed to the 100th percentile. The ROC metrics of β were identical to their counterparts in Table 1 because the optimal percentile cut-off was set at the 100th percentile. Here, β again had the best AUC (0.702), accuracy (0.645), and sensitivity (0.620), whereas α had the best specificity (0.842).

As the optimal percentile cut-off was determined to be the same as the one used in the entire-ROI-based analysis (i.e., 100th percentile) for β, we assessed the performance

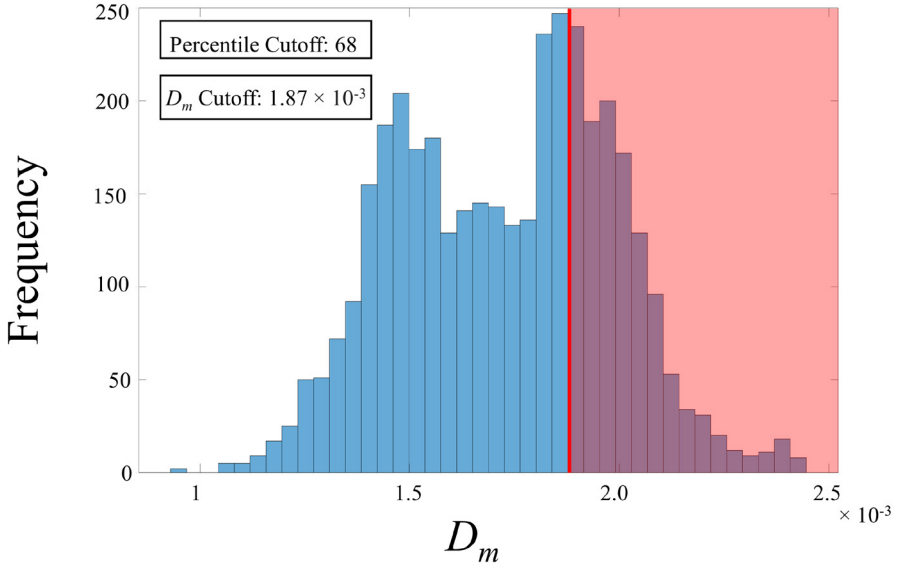

Fig. 2. A representative histogram of D_m values from the ROI of a grade II glioma patient. The dark-red line indicates the optimal percentile cut-off, in this case, the 68th percentile. All values in the shaded areas in pink were excluded from analysis.

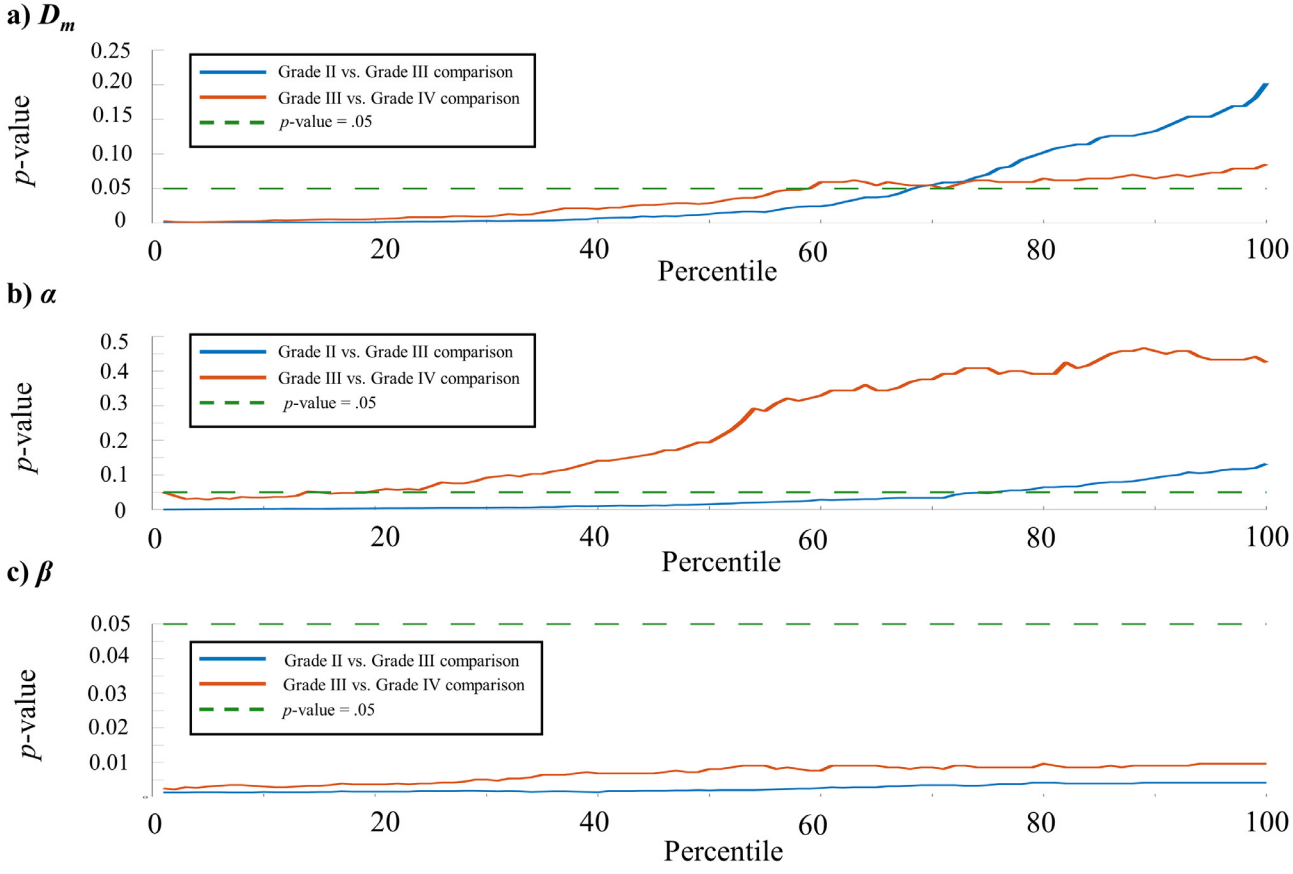

Fig. 3. Graphs of P value versus percentile for D_m, α, and β. The blue and orange curves are for differentiation between grade II and grade III, and grade III and IV gliomas, respectively. The dashed green line indicates P-value = 0.05.

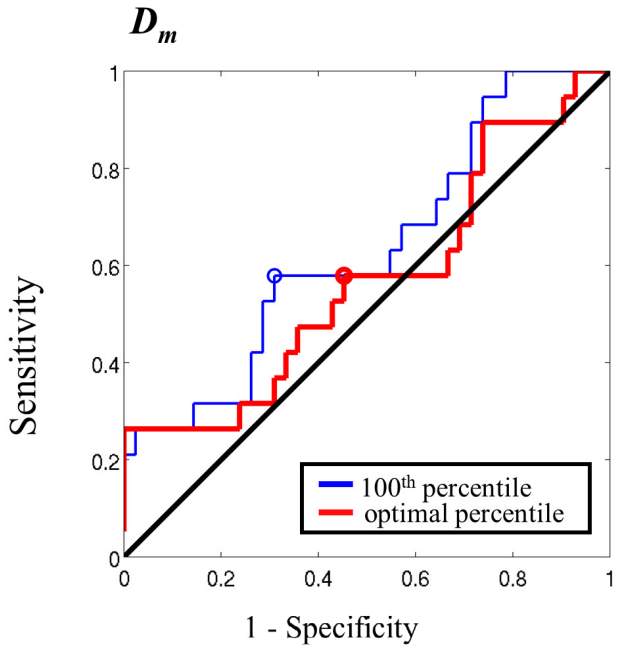

a

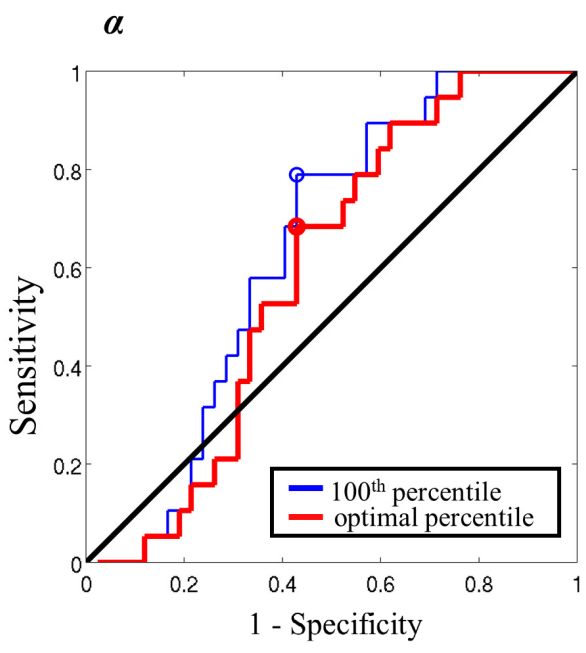

b

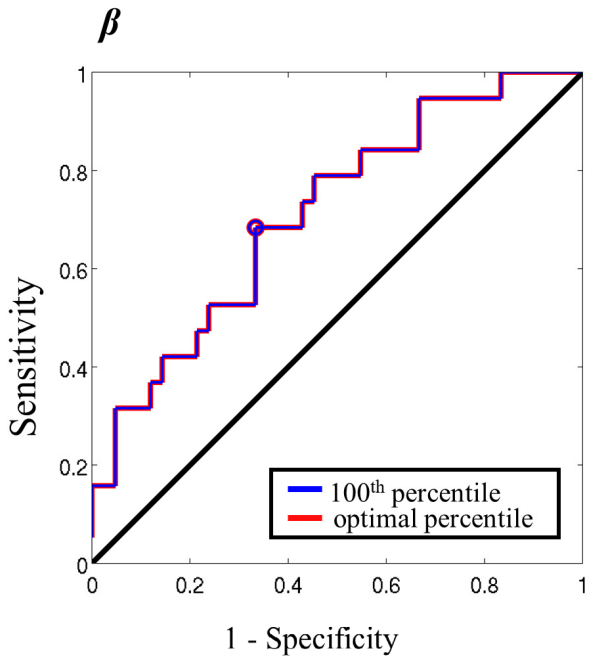

c

Fig. 4. ROC performance curves when using individual CTRW parameters to differentiate grade II from grade III gliomas. Results based on D_m, α, and β are shown in (a-c), respectively. Each plot displays the curves generated by using both the optimal percentile cut-off (in blue) and the 100th percentile (in red). Note that for β, the optimal percentile cut-off was chosen as the 100th percentile. Performance metrics are provided in Table 1.

of the (D_m, α) combination in differentiating between glioma grades by using a multivariable logistic regression, as summarized in Figure 6 and Table 3. Compared to the performance obtained from using the entire ROI (i.e., 100th percentile), the optimal percentile-based method was better in all metrics, sensitivity (0.761 vs. 0.690, P ≤ 0.05), specificity (0.578 vs. 0.526), accuracy (0.704 vs. 0.639, P ≤ 0.05), and AUC (0.671 vs. 0.599, P ≤ 0.05), in the differentiation between grades II and III as summarized in the first column of Table 3. As summarized in the second column of Table 3, for the differentiation between grades III and IV, the optimal percentile-based (D_m, α) combination

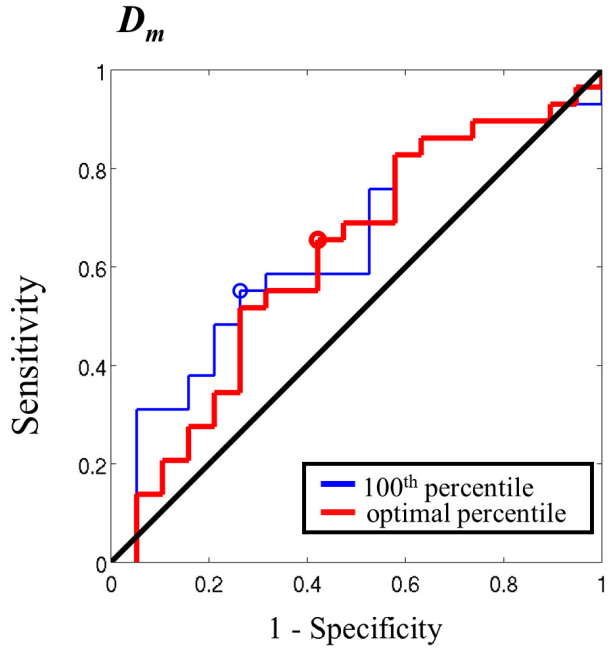

a

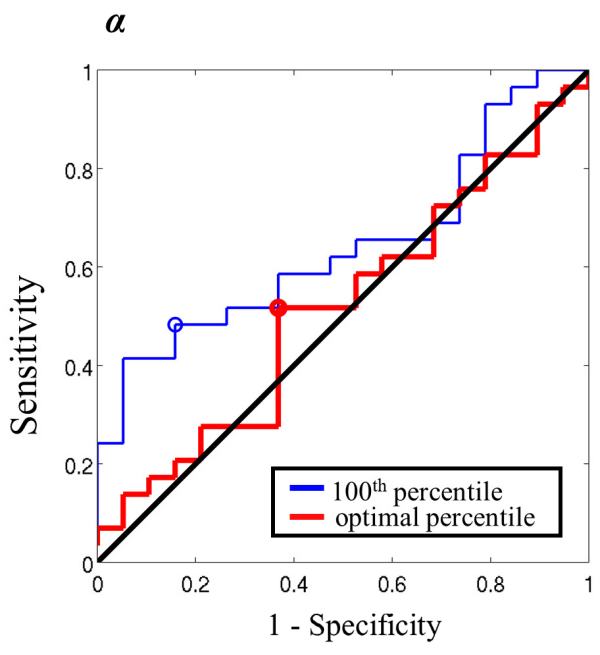

b

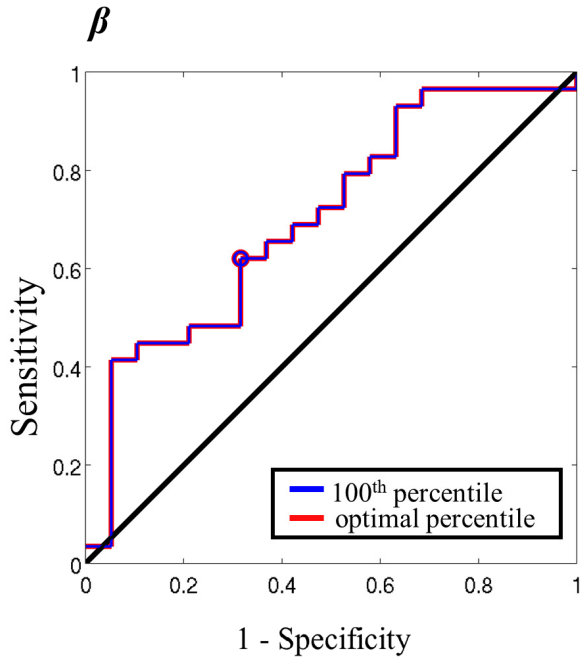

c

Fig. 5. ROC performance curves for differentiating grade III from grade IV tumors when using D_m, α, and β. The curves using the optimal percentile cut-off are shown in blue, those using the 100th percentile are shown in red. Note that for β, the optimal percentile cut-off is the 100th percentile. Performance metrics are provided in Table 2.

outperformed the one based on the entire-ROI-based analysis in sensitivity (0.789 vs. 0.578, P ≤ 0.05). Although we also observed an improvement in AUC (0.637 vs. 0.620), the difference was not statistically significant.

DISCUSSION

Imaging-based glioma assessment is important in managing brain-tumor patients, despite the prevalence of histopathology analysis and the rising emphasis on molecular markers. Histopathology analysis relies on tissue

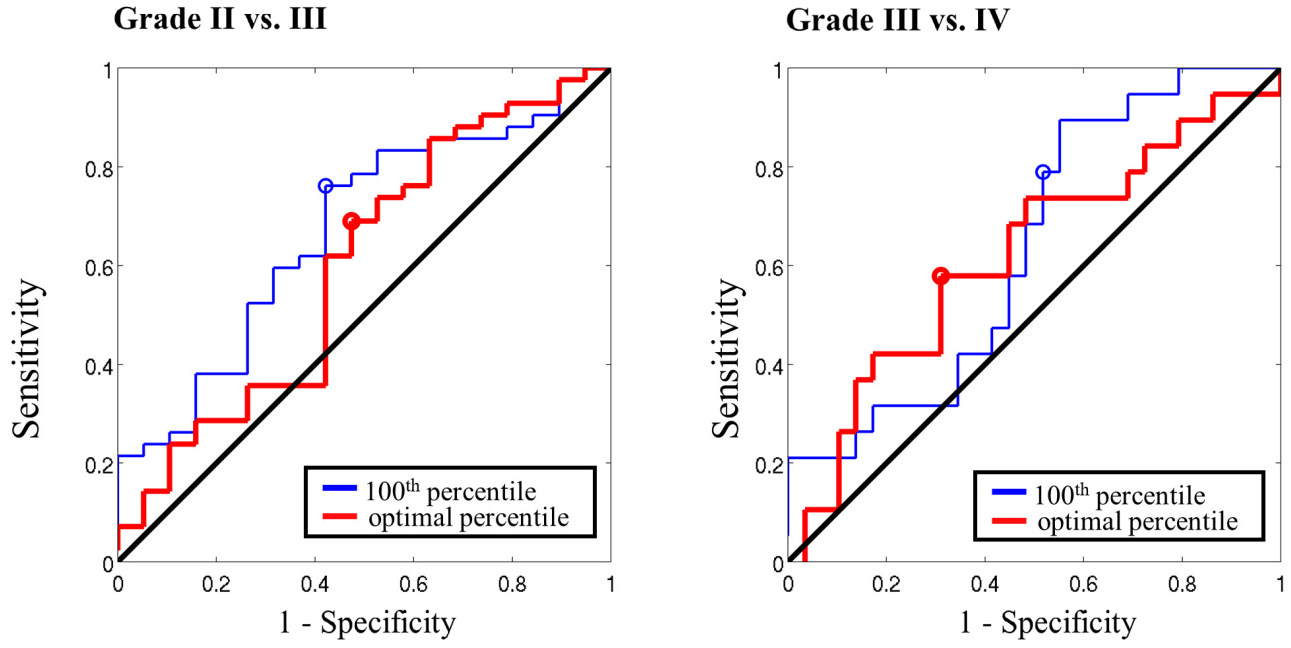

a b

Fig. 6. ROC performance curves using the combination of (D_m, α) to differentiate glioma grades. Differentiation of grade II vs. III in (a) and grade III vs. IV in (b). The curve using the optimal percentile cut-off is shown in blue, the curve using the 100th percentile in red. Performance metrics are summarized in Table 3.

Table 2. Receiver Operating Characteristic Performance Metrics of Each CTRW (Continuous-time random-walk) Parameter for Grades III and IV Differentiation Using an Optimal Percentile-Based Histogram Analysis and the Entire-ROI-Based (i.e., 100th percentile) analysis

	Optimal percentile-based histogram analysis		
	D_m	α	β
Sensitivity	0.551	0.482	0.620
Specificity	0.736*	0.842*	0.684
Accuracy	0.625	0.625	0.645
AUC	0.644	0.644	0.702
	Entire-ROI-based analysis		
Sensitivity	0.655	0.517	0.620
Specificity	0.578*	0.631*	0.684
Accuracy	0.625	0.562	0.645
AUC	0.618	0.519	0.702

Analysis in the upper half of the table is based on the mean parameter values computed from the an optimal percentile as described in the text. Analysis in the lower half of the table is based on the mean parameter values computed from the entire ROI.

Asterisk (*) indicates statistical significance between the performance metrics obtained from the optimal percentile- and entire-ROI-based analysis according to the McNemar test for specificity, sensitivity, and accuracy and the Hanley and McNeil test for AUC.

Table 3. Receiver Operating Characteristic Performance Metrics from the Combination of (D_m, α) for Differentiation of Grade II vs. III and Grade III vs. IV Gliomas. Parameter Values were Chosen Via an Optimal Percentile cut-off or 100th Percentile, Calculated Based on a Multivariable Logistic Regression

	Grade II vs. III	Grade III vs. IV
	Optimal percentile-based histogram analysis	
Sensitivity	0.761*	0.789*
Specificity	0.578	0.482
Accuracy	0.704*	0.604
AUC	0.671*	0.637
	Entire-ROI-based analysis	
Sensitivity	0.690*	0.578*
Specificity	0.526	0.689
Accuracy	0.639*	0.645
AUC	0.599*	0.620

Analysis in the upper half of the table is based on the mean parameter values computed from an optimal percentile as described in text. Analysis in the second half of the table is based on the mean parameter values computed from the entire ROI.

Asterisk (*) indicates statistical significance between the performance metrics obtained from the optimal percentile- and entire-ROI-based analysis according to the McNemar test for specificity, sensitivity, and accuracy and Hanley and the McNeil test for AUC.

specimens taken at a limited number of spatial locations and is thereby subject to sampling errors. Molecular markers also rely on tissue specimens and may fail due to an insufficient amount of tissue. In addition, tumors at or near specific locations, such as the brain stem in pediatric patients, present considerable surgical risks for biopsy or resection. In contrast, imaging-based glioma evaluation can sample the entire lesion non-invasively, no matter the tumor location. This advantage, however, also brings about a practical challenge: that of effectively and optimally analyzing the vast amount of voxel-level, spatially resolved data. Commonly, an ROI-based analysis yields a mean value from the entire ROI. This approach faces at least two limitations. First, the selection of an ROI depends on the operator and can be highly subjective. Second, when tumor tissue is heterogeneous, as in a glioma, where tumor, hemorrhage, necrosis, edema, and other pathologies can co-exist, the ROI-based approach can dilute contributions from the tumor tissue due to the averaging with other tissue components, reducing the sensitivity. This bias may explain why most DWI-based results are effective only for separating low- from high-grade gliomas, but not as effective for differentiating individual glioma grades (9). This bias may also account for the discrepancies between some published studies (7, 43, 44). To address these limitations, a quartile- or percentile-based approach has been proposed, in which only a specific percentile of the histogram computed within an ROI is used in order to filter out non-contributing tissue components (e.g., hemorrhage, necrosis, and/or edema) (33, 37, 45, 46). The selection of a quartile or a percentile of an ROI-based histogram has been somewhat arbitrary. In this study, we have addressed this issue in a systematic way by calculating an optimal percentile cut-off using a CTRW diffusion model as an example. We have investigated and determined the optimal percentile cut-offs for each of the three CTRW model parameters in order to differentiate grade II vs. grade III and grade III vs. grade IV gliomas. Importantly, we have demonstrated that glioma grading was improved when using the optimal percentile cut-offs than by averaging over the entire ROI. Our results can serve as a prototype for investigating other DWI-based quantitative parameters or non-diffusion-based parameters for glioma grading. The method described herein can also be extended beyond gliomas to other cancers.

Our previous studies have shown that the CTRW model parameters yielded lower values in tumors with higher grades (26, 46). In this study, we used the left tails of the parameter histograms (i.e., lower parameter values) to compute the optimal mean parameters by using the values that fell between 0% and the percentile cut-off. This strategy is consistent with the histopathology practice where the most malignant components of the specimen are used to make a diagnosis. We have observed that the optimal percentile cut-offs differ greatly among the three CTRW parameters. For example, to separate grade III from grade IV gliomas, the optimal percentile cut-offs ranged from 19% for α, 58% for D_m, to 100% for β, perhaps because of the different roles of these parameters in revealing the underlining tissue structural differences in the different grades of gliomas. Similar to ADC, D_m has been predominantly associated with tissue cellularity. The presence of necrosis, hemorrhage, and edema can substantially affect D_m through alterations in cellularity. As the tumor grade increases from II to IV, these confounding factors play an increasingly important role. Hence, the need for filtering out these perturbations within the tumor ROI increases. This explains why the optimal percentile cut-off decreased from 68% for grade II vs. grade III differentiation to 58% for grade III vs. grade IV differentiation (note that a lower percentile indicates more filtration). Unlike D_m, α and β have been associated with intravoxel tissue heterogeneities (23, 26, 28, 47, 48). It is important to recognize that microscopic (i.e., intravoxel) tissue heterogeneity can be influenced by macroscopic (i.e., intervoxel) tissue heterogeneity. Although heterogeneities at these two different spatial scales may not be completely separable, using an optimal percentile cut-off can be a practical way to filter out certain types of macroscopic heterogeneities, such as those introduced by tissue components other than those of the tumor itself. It is well known that macroscopic tissue heterogeneity increases with the tumor grade. Thus, the optimal percentile cut-offs of α are expected to be higher (i.e., less filtration) for differentiating grade II vs. grade III than for differentiating grade III vs. grade IV (i.e., more filtration), as we observed in our study (Fig. 3). It is worth noting that β behaved differently in glioma grading as measured by P-values. The entire histogram of β contributed to glioma grading without filtration, whereas α was substantially filtered out for grade III vs. grade IV differentiation. Although this observation is consistent with some published studies that have shown better performance of β over α (27, 46), the exact histologic underpinning is not known and should be investigated in future validation studies.

In general, the approach with optimal percentile cut-offs outperformed the traditional method of computing

the mean over the entire ROI (Figs. 4-6, Tables 1-3). The improvement was observed not only on individual CTRW parameters, but also in the combination of D_m and α as evidenced by AUC and other statistical parameters. The use of multiple parameters can integrate several aspects of the underlying changes in glioma tissues and thus improve the performance, as other studies have shown (26, 27, 30).

In this study, we focused on pair-wise differentiations between neighboring glioma grades (grade II vs. grade III, grade III vs. grade IV), largely because grade II vs. grade IV differentiation is typically less challenging. The proposed technique can be generalized to a finer classification of the glioma grades, which would allow identification of the grades among all tumors. However, such differentiation would require a more balanced sample size among all three grades. Future studies should investigate the feasibility of the proposed technique for a more detailed classification of the glioma grades with a larger cohort.

Our study has limitations. First, although most of our results suggest that the approach with optimal percentile cut-offs is advantageous, the approach did not yield the expected outcome in two scenarios where the optimal percentile cut-off produced lower sensitivities than did the entire-ROI analysis in differentiating between grade III and IV tumors when the CTRW parameters were used individually and produced lower specificities when they were used conjointly. This unexpected finding may have resulted from the inadequate sample size, sub-optimal signal-to-noise ratio in the parameter maps, or other factors requiring further investigation. Second, our study was limited to a single diffusion model - the CTRW model. To generalize the proposed approach with optimal percentile cut-offs, other diffusion models, such as intravoxel incoherent motion (IVIM) (49), diffusion kurtosis imaging (DKI) (18), q-space trajectory imaging (QTI) (14), or restricted spectrum imaging (RSI) (22), need to be investigated in the context of tumor grading or other applications. Third, the specific percentile cut-off values obtained in this study were intended only to demonstrate the method and should not be used as suggested values for clinical evaluations. To validate these cut-off values, a larger sample of patients would be required.

Last, our analysis did not include patients with grade I gliomas due to their low rate of clinical presentation in adults. Despite these limitations, the approach illustrated in this study provides a systematic way to analyze ROI-based data for glioma grading in specific and tissue characterization in general.

In conclusion, by employing the CTRW diffusion model as an example, we have shown that a percentile-based analysis can outperform the conventional ROI-based methods in differentiating individual glioma grades. The proposed approach provides a systematic way to statistically determine a cut-off in the percentile analysis of diffusion MRI parameters. With its ability to mitigate the issues associated with manual ROI selection and volume averaging over a heterogenous ROI, the technique presented in this study is expected to find other applications in cancer imaging where quantitative diffusion parameters are used as imaging markers.

Acknowledgments

We are grateful to Jingjing Jiang, Rifeng Jiang, and Changliang Su for assisting with MRI image collections, to Dr. Liping Qi, Dr. Tibor Valyi-Nagy, Dr. Kaibao Sun, and Dr. Qingfei Luo and Guangyu Dan for helpful discussions, and to Dong Kuang for guidance on pathology.

REFERENCES

1. Louis DN, Perry A, Reifenberger G, et al. The 2016 World Health Organization Classification of tumors of the central nervous system: a summary. Acta Neuropathol 2016;131:803-820
2. Ostrom QT, Gittleman H, Stetson L, Virk SM, Barnholtz-Sloan JS. Epidemiology of gliomas. Cancer Treat Res 2015;163:1-14
3. Ludwig K, Kornblum HI. Molecular markers in glioma. J Neurooncol 2017;134:505-512
4. Ginsberg LE, Fuller GN, Hashmi M, Leeds NE, Schomer DF. The significance of lack of MR contrast enhancement of supratentorial brain tumors in adults: histopathological evaluation of a series. Surg Neurol 1998;49:436-440
5. Al-Okaili RN, Krejza J, Woo JH, et al. Intraaxial brain masses: MR imaging-based diagnostic strategy--initial experience. Radiology 2007;243:539-550
6. van Dijken BRJ, van Laar PJ, Holtman GA, van der Hoorn A. Diagnostic accuracy of magnetic resonance imaging techniques for treatment response evaluation in patients with high-grade glioma, a systematic review and meta-analysis. Eur Radiol 2017;27:4129-4144
7. Zonari P, Baraldi P, Crisi G. Multimodal MRI in the characterization of glial neoplasms: the combined role of single-voxel MR spectroscopy, diffusion imaging and echo-planar perfusion imaging. Neuroradiology 2007;49:795-803

8. Kickingereder P, Wiestler B, Sahm F, et al. Primary central nervous system lymphoma and atypical glioblastoma: multiparametric differentiation by using diffusion-, perfusion-, and susceptibility-weighted MR imaging. Radiology 2014;272:843-850
9. Zhang L, Min Z, Tang M, Chen S, Lei X, Zhang X. The utility of diffusion MRI with quantitative ADC measurements for differentiating high-grade from low-grade cerebral gliomas: evidence from a meta-analysis. J Neurol Sci 2017;373:9-15
10. Le Bihan D, Iima M. Diffusion magnetic resonance imaging: what water tells us about biological tissues. PLoS Biol 2015;13:e1002203
11. Le Bihan D. Apparent diffusion coefficient and beyond: what diffusion MR imaging can tell us about tissue structure. Radiology 2013;268:318-322
12. Tang L, Zhou XJ. Diffusion MRI of cancer: from low to high b-values. J Magn Reson Imaging 2019;49:23-40
13. Niendorf T, Dijkhuizen RM, Norris DG, van Lookeren Campagne M, Nicolay K. Biexponential diffusion attenuation in various states of brain tissue: implications for diffusion-weighted imaging. Magn Reson Med 1996;36:847-857
14. Assaf Y, Mayk A, Cohen Y. Displacement imaging of spinal cord using q-space diffusion-weighted MRI. Magn Reson Med 2000;44:713-722
15. Yablonskiy DA, Bretthorst GL, Ackerman JJ. Statistical model for diffusion attenuated MR signal. Magn Reson Med 2003;50:664-669
16. Bennett KM, Schmainda KM, Bennett RT, Rowe DB, Lu H, Hyde JS. Characterization of continuously distributed cortical water diffusion rates with a stretched-exponential model. Magn Reson Med 2003;50:727-734
17. Le Bihan D, Breton E, Lallemand D, Aubin ML, Vignaud J, Laval-Jeantet M. Separation of diffusion and perfusion in intravoxel incoherent motion MR imaging. Radiology 1988;168:497-505
18. Jensen JH, Helpern JA, Ramani A, Lu H, Kaczynski K. Diffusional kurtosis imaging: the quantification of non-gaussian water diffusion by means of magnetic resonance imaging. Magn Reson Med 2005;53:1432-1440
19. Özarslan E, Basser PJ, Shepherd TM, Thelwall PE, Vemuri BC, Blackband SJ. Observation of anomalous diffusion in excised tissue by characterizing the diffusion-time dependence of the MR signal. J Magn Reson 2006;183:315-323
20. Westin CF, Knutsson H, Pasternak O, et al. Q-space trajectory imaging for multidimensional diffusion MRI of the human brain. Neuroimage 2016;135:345-362
21. Panagiotaki E, Chan RW, Dikaios N, et al. Microstructural characterization of normal and malignant human prostate tissue with vascular, extracellular, and restricted diffusion for cytometry in tumours magnetic resonance imaging. Invest Radiol 2015;50:218-227
22. White NS, Leergaard TB, D'Arceuil H, Bjaalie JG, Dale AM. Probing tissue microstructure with restriction spectrum imaging: histological and theoretical validation. Hum Brain Mapp 2013;34:327-346
23. Zhou XJ, Gao Q, Abdullah O, Magin RL. Studies of anomalous diffusion in the human brain using fractional order calculus. Magn Reson Med 2010;63:562-569
24. Magin RL, Abdullah O, Baleanu D, Zhou XJ. Anomalous diffusion expressed through fractional order differential operators in the Bloch-Torrey equation. J Magn Reson 2008;190:255-270
25. Ingo C, Magin RL, Colon-Perez L, Triplett W, Mareci TH. On random walks and entropy in diffusion-weighted magnetic resonance imaging studies of neural tissue. Magn Reson Med 2014;71:617-627
26. Karaman MM, Sui Y, Wang H, Magin RL, Li Y, Zhou XJ. Differentiating low- and high-grade pediatric brain tumors using a continuous-time random-walk diffusion model at high b-values. Magn Reson Med 2016;76:1149-1157
27. Karaman MM, Wang H, Sui Y, Engelhard HH, Li Y, Zhou XJ. A fractional motion diffusion model for grading pediatric brain tumors. Neuroimage Clin 2016;12:707-714
28. Barrick TR, Spilling CA, Ingo C, et al. Quasi-diffusion magnetic resonance imaging (QDI): a fast, high b-value diffusion imaging technique. Neuroimage 2020;211:116606
29. Ingo C, Sui Y, Chen Y, Parrish TB, Webb AG, Ronen I. Parsimonious continuous time random walk models and kurtosis for diffusion in magnetic resonance of biological tissue. Front Phys 2015;3
30. Sui Y, Wang H, Liu G, et al. Differentiation of low- and high-grade pediatric brain tumors with high b-value diffusion-weighted MR imaging and a fractional order calculus model. Radiology 2015;277:489-496
31. Sui Y, Xiong Y, Jiang J, et al. Differentiation of low- and high-grade gliomas using high b-value diffusion imaging with a non-Gaussian diffusion model. AJNR Am J Neuroradiol 2016;37:1643-1649
32. Tang L, Sui Y, Zhong Z, et al. Non-Gaussian diffusion imaging with a fractional order calculus model to predict response of gastrointestinal stromal tumor to second-line sunitinib therapy. Magn Reson Med 2018;79:1399-1406
33. Karaman MM, Tang L, Li Z, Sun Y, Li JZ, Zhou XJ. In vivo assessment of Lauren classification for gastric adenocarcinoma using diffusion MRI with a fractional order calculus model. Eur Radiol 2021;31:5659-5668
34. Cha S. Update on brain tumor imaging: from anatomy to

physiology. AJNR Am J Neuroradiol 2006;27:475-487
35. Just N. Improving tumour heterogeneity MRI assessment with histograms. Br J Cancer 2014;111:2205-2213
36. Padhani AR, Liu G, Koh DM, et al. Diffusion-weighted magnetic resonance imaging as a cancer biomarker: consensus and recommendations. Neoplasia 2009;11:102-125
37. Kang Y, Choi SH, Kim YJ, et al. Gliomas: histogram analysis of apparent diffusion coefficient maps with standard- or high-b-value diffusion-weighted MR imaging--correlation with tumor grade. Radiology 2011;261:882-890
38. Huang H, Zhang Y, Cheng J, Wen M. Whole-tumor histogram analysis of apparent diffusion coefficient maps in grading diagnosis of ependymoma. Chinese J Acad Radiol 2020;2:41-46
39. Chenevert TL, Malyarenko DI, Galban CJ, et al. Comparison of voxel-wise and histogram analyses of glioma ADC maps for prediction of early therapeutic change. Tomography 2019;5:7-14
40. Sorensen AG, Buonanno FS, Gonzalez RG, et al. Hyperacute stroke: evaluation with combined multisection diffusion-weighted and hemodynamically weighted echo-planar MR imaging. Radiology 1996;199:391-401
41. Fagerland MW, Lydersen S, Laake P. The McNemar test for binary matched-pairs data: mid-p and asymptotic are better than exact conditional. BMC Med Res Methodol 2013;13:91
42. Hanley JA, McNeil BJ. A method of comparing the areas under receiver operating characteristic curves derived from the same cases. Radiology 1983;148:839-843
43. Catalaa I, Henry R, Dillon WP, et al. Perfusion, diffusion and spectroscopy values in newly diagnosed cerebral gliomas. NMR Biomed 2006;19:463-475
44. Murakami R, Hirai T, Sugahara T, et al. Grading astrocytic tumors by using apparent diffusion coefficient parameters: superiority of a one- versus two-parameter pilot method. Radiology 2009;251:838-845
45. Tozer DJ, Jager HR, Danchaivijitr N, et al. Apparent diffusion coefficient histograms may predict low-grade glioma subtype. NMR Biomed 2007;20:49-57
46. Karaman MM, Zhang J, Xie KL, Zhu W, Zhou XJ. Quartile histogram assessment of glioma malignancy using high b-value diffusion MRI with a continuous-time random-walk model. NMR Biomed 2021;34:e4485
47. Zhong Z, Merkitch D, Karaman MM, et al. High-spatial-resolution diffusion MRI in Parkinson disease: lateral asymmetry of the substantia nigra. Radiology 2019;291:149-157
48. Yu Q, Reutens D, Vegh V. Can anomalous diffusion models in magnetic resonance imaging be used to characterise white matter tissue microstructure? Neuroimage 2018;175:122-137
49. Le Bihan D, Breton E, Lallemand D, Grenier P, Cabanis E, Laval-Jeantet M. MR imaging of intravoxel incoherent motions: application to diffusion and perfusion in neurologic disorders. Radiology 1986;161:401-407